Application of Flow Battery in Marine Current Turbine System for Daily Power Management

Zhibin Zhou[1,2,3], Franck Scuiller[1], Jean Frédéric Charpentier[1]
[1]French Naval Academy, EA 3634 IRENav, Brest, France
Email: zhibin.zhou@ecole-navale.fr

Mohamed Benbouzid[2] and Tianhao Tang[3]
[2]University of Brest, EA 4325 LBMS, Brest, France
[3] Shanghai Maritime University, Shanghai, China
Email: Mohamed.Benbouzid@univ-brest.fr, thtang@shmtu.edu.cn

***Abstract*—Predictable tidal current resources make marine current turbine (MCT) generation system highly attractive as an electricity supply source for coastal areas and remote islands. However, the tidal speed varies greatly due to the flood and ebb tides during one day period. This results large mismatch between MCT produced power and grid-side (or load-side) demanded power. This paper focuses on a grid-connected MCT system and proposes using vanadium redox flow battery (VRB) energy storage system to manage the combined output power and to follow grid-side demand on a daily basis. The VRB model and parameter calculation process are detailed in this paper. The diesel generator (DG) system is considered as a backup power supply source in case of low battery state of charge (SoC) caused by losses during long-time battery operation.**

Simulations are carried-out on a grid-connected MCT system with VRB ESS to follow a given power demand profile during one day period. The results valid the proposed VRB sizing and control strategy. The DG system is demonstrated as a feasible solution to avoid VRB reaching its low SoC limitation and to guarantee the expected power injection to the local grid.

***Keywords*—Marine current turbine, flow battery modeling, grid power demand, energy storage.**

I. Introduction

Highly predictable tidal resources and high energy density due to sea water density make marine current turbine (MCT) system very attractive for development. In recent years, various turbine technologies have been researched and tested to harness kinetic energy from marine tidal currents [1-2]. The astronomic nature of tides cause seawater motion regularly each day with a period of approximately 12 h and 24 min (a semidiurnal tide), or with a period of about 24 h and 48 min (a diurnal tide). This tidal movement causes the variation of tide current speed and thus resulting large MCT output power variation during one day. Moreover, during some periods when the current speed is too low (< 1m/s), the MCT is unable to produce power due to the system inertia and mechanical losses.

On the other hand, the electricity demand from the grid side (or consumer side) has its own pattern during each day. Large difference between the power produced from the renewable sources and the demanded power from the grid side could cause frequency variation and instability problems for the grid [3]. Various energy storage systems (ESS) have been studied for the MCT application in [4], and the flow battery technology has been found very suitable for hours energy storage due to deep discharge ability, long service life and flexibility power/energy sizing.

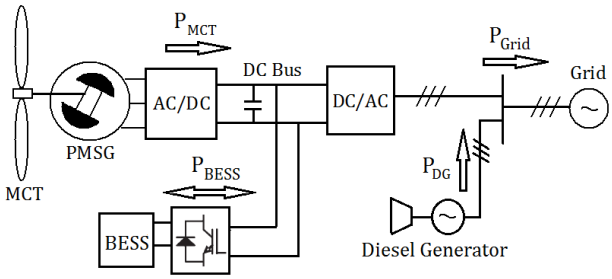

Fig. 1. General scheme for a grid-connected MCT system with BESS.

In this paper, one grid-connected MCT generation system with battery energy storage system (BESS) is studied to follow a given power demand profile on daily basis. Figure 1 shows the general system structure. The BESS is connected to the DC bus of the back-to-back PWM converter which interfaces the permanent magnet synchronous generator (PMSG) and the grid. The diesel generator (DG) in Fig. 1 serves as a backup power supply source for enhancing grid demand power following ability.

In Section II, the MCT power characteristic and the typical load demand on one day basis are described. In Section III, the flow battery modeling and the parameter calculation are presented. In Section IV, the battery control strategy and the simulations with and without diesel generator are presented. The conclusion is then given in Section V.

II. Marine Current Turbine Power Characteristic

For MCTs, the power extracting principles are similar to wind turbines. The power produced by a horizontal-axis MCT can be calculated by the following equation.

$$P_{\mathrm{MCT}} = \frac{1}{2}\rho C_p \pi R^2 V_{\mathrm{tide}}^3 \quad (1)$$

This work is supported by Brest Métropole Océane (BMO) and the Shanghai Maritime University.

In (1), the sea water density ρ and the turbine radius R are considered as constants; V_{tide} is the tidal current velocity; C_p is the turbine power coefficient which depends on the turbine blade structure and hydrodynamics. For typical turbine designs, the optimal C_p value for normal operation is estimated to be in the range of 0.35-0.5 [5]. For a given turbine, the C_p curve can be approximated as a function of the tip speed ratio (λ) and the blade pitch angle (β) based on the experimental results [6]. The C_p curve used in this paper is shown by Fig. 2 (β = 0 for the fixed-blade case).

In this paper, the direct-driven MCT is supposed to have a power rating of 1.5 MW. The maximum rotor speed to follow MPPT is 25 rpm (2.62 rad/s) corresponding to a tidal current speed of 3.2 m/s. When the tidal current exceeds 3.2 m/s, the MCT harnessed power can be limited to 1.5 MW by power limitation strategies described in [7]. Figure 3 shows the MCT extractable powers under different tidal current speeds, which are calculated based on the C_p curve and (1).

Figure 4 shows an example for tidal current speed, the corresponding MCT harnessed power, and the grid power demand profile on one day period. The cubic relationship between the tidal current velocity and the turbine power makes the MCT produce high power at both flooding tide and ebb tide crests. In the middle of these tide crests, when the tidal current velocity is lower than 1 m/s, the MCT is unable to produce power. The supposed grid-injection power (P_{Grid} in Fig. 4b) reference can be calculated based on typical load curves [8] and the average MCT power during one day. From

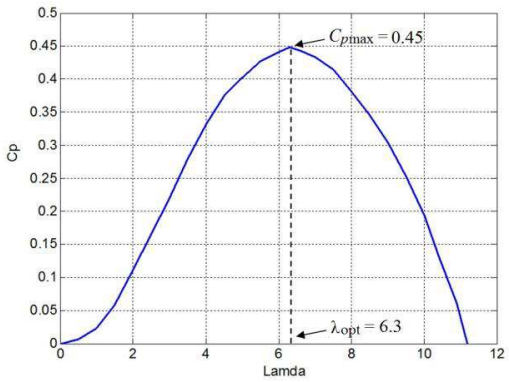

Fig. 2. C_p curve of the MCT.

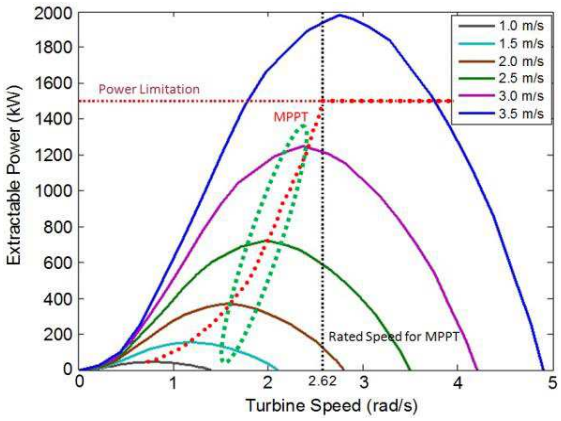

Fig. 3. The MCT power under different tidal current speeds.

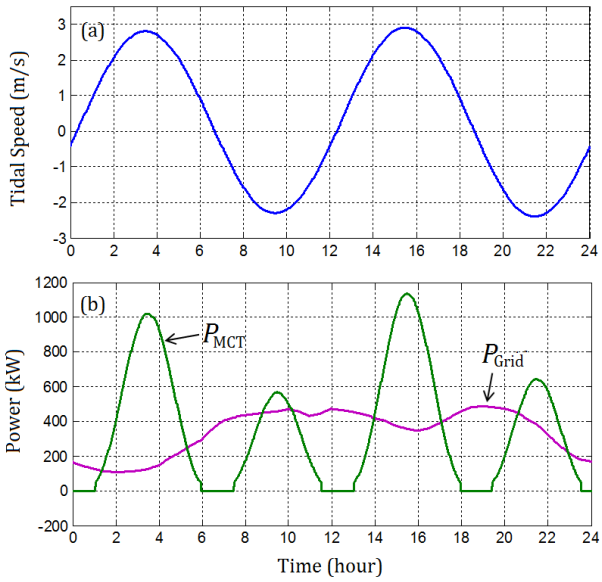

Fig. 4. Typical case for one day: (a) tidal current speed, (b) MCT produced power and grid demand power.

Fig. 4(b), it can be seen that during the peak load periods (10h-12h and 18h-20h) the MCT may produce low power or can not produce power due to low tidal current velocity. Therefore, energy storage system is needed to store excessive energy during MCT peak power periods and to inject the stored energy to the grid side during peak load periods.

The MCT and BESS system output is supposed to follow the grid demand on a daily basis. The maximum difference between the MCT power and the grid demand power during one day period can be considered as the power rating of the BESS; and the maximum energy variation (calculated by integrating the power difference shown in Fig.4b) can serve as a basic estimation of the minimum required BESS energy capacity. In this case, the BESS system in this paper is sized with a power rating of 1MW and an energy capacity of 3MWh.

III. Flow Battery Modeling

A. Flow Battery Equivalent Circuit Model

Flow battery technology is developed for high energy capacity applications over the past 20 years. This technology uses two external tanks to reserve liquid electrolytes and a pump system for circulating the electrolytes to the battery cell stack (consisting of the two electrodes and the ion exchange membrane) [9]. The distinguished advantage of flow batteries is flexible energy and power sizing, long service life, deep discharge ability and low maintenance.

The vanadium redox flower battery (VRB) is considered in this paper. The equivalent circuit model is proposed in [10] and used by other researchers [11], however some parameter calculations are not detailed and the battery standby mode is not considered.

Figure 5 shows the model in this paper, the stack current (I_{stack}) and stack voltage (V_{stack}) represent the battery cell-stack current and the internal battery electromotive force; and

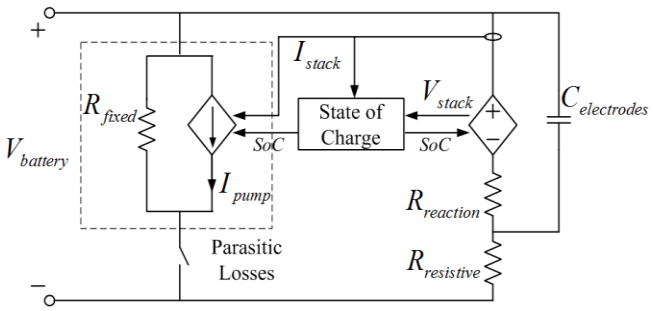

Fig. 5. VRB equivalent circuit model [11].

these two terms will be used to calculate the battery state of charge (SoC). The battery terminal voltage and current are expressed as $V_{battery}$ and $I_{battery}$. The internal resistance ($R_{reaction}$ and $R_{resistive}$) are modeled for reaction kinetics loss, mass transport resistance, membrane resistance, electrode resistance and bipolar plate resistance. The transient component associated with the electrode capacitance is modeled by $C_{eletrodes}$. The parasitic resistance R_{fixed} allows modeling the stack by-pass current. The power losses due to the circulation pump and the system controller are represented by the losses current I_{pump} . The switch on the parasitic branch of the equivalent circuit will be turned on when the battery is in operation (charge or discharge) and turned off when the battery is in standby mode.

B. Parameter Estimation Process for the VRB Model

The battery stack voltage represents the internal battery electromotive force. The value is directly related to the battery SoC as follows.

$$V_{stack} = n \cdot \left(1.4 + k \ln\left(\frac{SoC}{1-SoC}\right)\right) \tag{2}$$

In (2), n is number of cells in series in the battery stack; 1.4 is the nominal battery electromotive force for one cell; k is a coefficient relating to the temperature and can take a value of 0.0514 at 25℃. The terminal battery voltage can be calculated from Fig. 5 as

$$V_{battery} = V_{stack} + I_{stack}(R_{reaction} + R_{resistive}) \tag{3}$$

It should be noted that the I_{stack} takes the positive value for the charge mode and negative value for the discharge mode in this paper. The battery terminal current has the same direction as the I_{stack} and can be obtained considering the parasitic losses as

$$I_{battery} = I_{stack} + \left(\frac{V_{battery}}{R_{fixed}} + I_{pump}\right) \tag{4}$$

The internal resistances ($R_{reaction}$ and $R_{resistive}$) and the parasitic resistance R_{fixed} can be estimated by the power losses at the rated battery discharge current and their values are generally constant during battery operational range.

The flow battery has about 79% efficiency at the operating point of rated discharge current I_{bmax} and 20% SoC. It can be estimated that for the nominal power loss ξ_N = 21% , 15% accounts for internal losses (ξ_1 and ξ_2 for losses on $R_{reaction}$ and $R_{resistive}$ respectively) and 6% accounts for parasitic losses (ξ_3 and ξ_4 for losses on R_{fixed} and I_{pump} respectively).

In order to enable the batter to provide the rated power P_N with a nominal loss ξ_N , the rated stack output power should be calculated by

$$P_{stackN} = \frac{P_N}{1-\xi_N} \tag{5}$$

For the fixed parasitic loss, the R_{fixed} can be calculated by

$$R_{fixed} = \frac{V_{b\min}^2}{\xi_3 \cdot P_{stackN}} \tag{6}$$

where $V_{b\min}$ is the minimum battery voltage defined at the rated discharge current $I_{b\max}$ (considering as the rated battery current). The relationship with the battery rated power is $P_N = V_{b\min} \times I_{b\max}$.

For the parasitic pump loss, it is related to the stack current and SoC as shown in (7)

$$P_{pump} = V_{battery} \times I_{pump} = k' \left(\frac{|I_{stack}|}{SoC}\right) \tag{7}$$

The constant k' can be estimated at the operating point of $I_{b\max}$. If the pump loss is estimated as two times as the fixed parasitic resistance loss at $I_{b\max}$ and 20% SoC, then the k' can be calculated by

$$k' = \frac{0.2\xi_4 P_{stackN}}{I_{b\max} + 3I'} \tag{8}$$

where the I' is the current through the fixed parasitic resistance at the operating point of $I_{b\max}$, and can be calculated by $I' = V_{b\min} / R_{fixed}$. Then the pump current I_{pump} can be calculated as follows.

$$I_{pump} = \frac{k'}{V_{b\min}} \left(\frac{|I_{stack}|}{SoC}\right) = \frac{0.2\xi_4 P_{stackN}}{P_N + 3\xi_3 P_{stackN}} \left(\frac{|I_{stack}|}{SoC}\right) \tag{9}$$

The internal resistances $R_{reaction}$ and $R_{resistive}$ can be calculated by (10) and (11) respectively.

$$R_{reaction} = \xi_1 P_{stackN} / \left(I_{b\max} + 3I'\right)^2 \tag{10}$$

$$R_{resistive} = \xi_2 P_{stackN} / \left(I_{b\max} + 3I'\right)^2 \tag{11}$$

The SoC of the battery is calculated as follows.

$$SoC_t = SoC_{t-1} + \Delta SoC \tag{12}$$

$$\Delta SoC = \frac{\Delta E}{E_N} = \frac{V_{stack} I_{stack} \Delta t}{P_N T_N} \tag{13}$$

where Δt is the calculation step; E_N is the energy capacity of the battery and T_N is the time duration for which the battery can provide P_N.

C. Charge-Discharge Characteristics for the VRB

The BESS in this paper is sized with a power rating of P_N = 1MW and energy capacity of E_N = 1MW×3h. The open-circuit battery voltage at 50% SoC is 1500V. It needs n = 1072 cells in series to make up the battery stack. The minimum battery terminal voltage is limited at V_{bmin} = 1170V and the rated discharge current is I_{bmax} = 855A. The power losses used to calculate the resistance and parameters in the battery model are set as : ξ_1 = 9%, ξ_2 = 6% , ξ_3 = 2% and ξ_4 = 4%. Each battery cell capacitance is about 6F, then the equivalent electrode capacitance for 1072 cells in series is calculated by $C_{eletrodes}$ = 6F/1072. The parameters for the VRB circuit model can be found in Appendix.

Figures 6 and 7 show the VRB battery used charge-discharge characteristics.

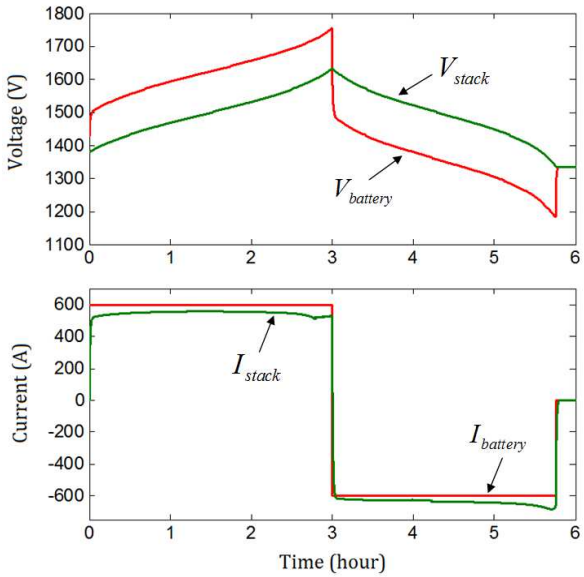

Fig. 6. VRB voltage and current variations during a charge-discharge cycle.

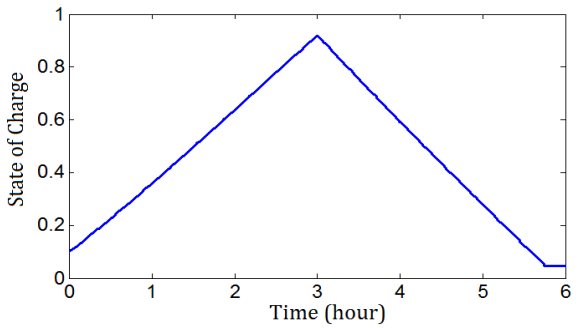

Fig. 7. VRB SoC variation during a charge-discharge cycle.

The battery is charged 3 hours with a constant current of 600A and a initial SoC of 0.1, and then discharged 3 hours later with the same absolute current value. From Fig. 6 it can be seen that at the switching instant from charge mode to discharge mode, the $V_{battery}$ is discontinuous due to the sudden voltage polarity change on the internal resistances. The difference between $I_{battery}$ and I_{stack} in Fig. 7 is caused by the parasitic current losses.

In this constant current charge-discharge cycle, the discharge mode can not last over 3 hours because of the battery losses. The battery should be turned off when the SoC is too low (at 5% SoC in Fig. 7). When the battery is turned off, the battery current will be zero and $V_{battery}$ will be equal to the battery internal electromotive force V_{stack} as shown in Fig. 6.

IV. MCT WITH FLOW BATTERY ENERGY STORAGE

A. System Configuration and BESS control scheme

The general system structure of the MCT with BESS was shown in Fig. 1. It should be noted that this paper focuses on the modeling and control of the BESS to enable the combined MCT and BESS power to follow the required grid power demand on daily basis.

The tidal current speed for one day used in this paper has been shown in Fig. 4(a). The MCT and generator system is modeled as a simple power source in this paper to calculate the MCT power profile according to (1). The MCT has a rated power of 1.5 MW and the DC bus voltage of the back-to-back converter is set to V_{dc} = 1500 V.

The diesel generator shown in Fig. 1 serves as a backup power source. For grid-connected case, diesel generators can be used to relieve grid burden during peak loads or provide emergency power supply during grid black out. In this paper, the diesel generator is modeled as a three-phase current source to provide powers when the battery SoC is too low.

The BESS is connected through a bi-directional DC/DC converter to the DC bus of the back-to-back converter as shown in Fig. 1. The power converters are modeled using average-value method in this paper for facilitating long-time period simulation. The principle of bi-directional buck-boost DC/DC converter [12] can be simplified as

$$\frac{V_{out}}{V_{in}} = \frac{D_d}{1 - D_u} = D \tag{14}$$

For the BESS, the V_{in} is the DC bus side voltage V_{dc} and the V_{out} is the battery terminal voltage $V_{battery}$; D is the voltage ratio decided by the switch duty ratios D_d and D_u. In the step-down mode, D_u = 0 and D_d is controlled in the [0,1]; while in the step-up mode, D_d = 1 and D_u is controlled in the [0,1]. The corresponding switches triggered to realize the duty ratios are determined by converter topology and the power flow direction. In this paper, the voltage ratio D serves as the control reference for the average-value converter model.

The battery reference power (positive for charge mode) is set to compensate the difference between the available power supply and grid power demand as follows.

$$P^*_{\text{BESS}} = P_{\text{MCT}} + P_{\text{DG}} - P^*_{\text{Grid}} \quad (15)$$

Figure 8 shows the BESS side DC/DC converter control scheme. In this control scheme, the voltage ratio D is limited in the range of $0.78V_{dc}$ and $1.2V_{dc}$ indicating the battery voltage is limited from 1170V to 1790V. The battery limit module in Fig. 8 is used to hold the value of D when the battery is turned off. The battery is supposed to turn off once the SoC tends to exceed the range of 0.1 and 1, or the absolute value of P_{BESS} reaches the rated value of P_N.

B. Simulation without the DG

The tidal current speed and the average MCT produced power during one day period are predictable. In this paper, the grid demand power is set to have an average value equals 90% average MCT produced power considering the system losses. The grid demand power profile (as shown in Fig. 4b) reflects the load variation during one day period.

In this section, only MCT and BESS are considered to provide grid demand power during one day. The 3MWh VRB model described in the previous section is integrated into the 1.5 MW MCT system. Figure 9 shows the MCT produced power, the power injected into the grid and the BESS power. Positive BESS power indicates the battery is charged and negative BESS power indicates battery is discharged. Figure 10 and 11 show the battery voltage/current and SoC variation. The initial battery SoC is set at 0.4. From Fig. 11, it can be seen that the battery SoC varies in the range of 0.11 and 0.91 and at the end of the day the SoC will decrease below 0.2. This SoC decreasing phenomenon is caused by the battery losses.

Figure 12 and 13 show the case when the initial SoC is set at 0.3. During 13:05-14:00 and 20:10-20:50, the SoC will reach its low limitation of 0.1 and the battery will be turned off.

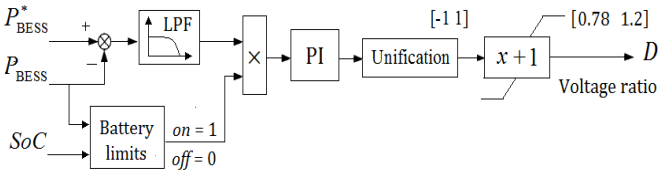

Fig. 8. Control scheme of the BESS side DC/DC converter.

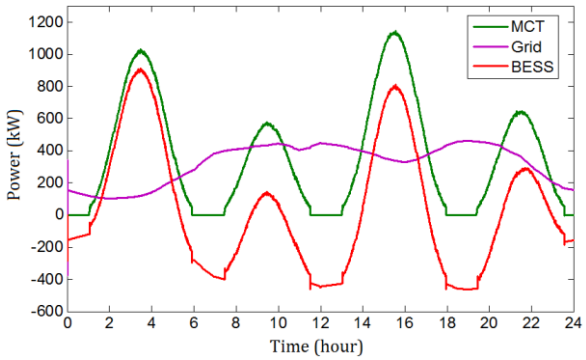

Fig. 9. Powers of the MCT system with BESS during one day.

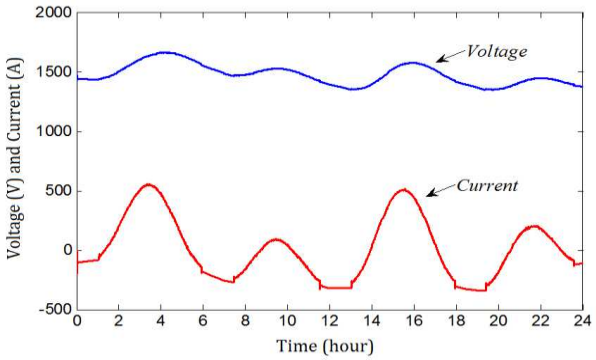

Fig. 10. BESS voltage and current.

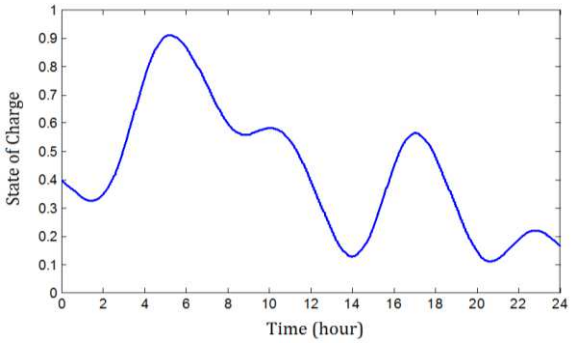

Fig. 11. SoC of the BESS.

When the battery is off, the P_{Grid} will drop to the P_{MCT} (shown in Fig. 12) and that means the grid power demand can not be satisfied. The battery voltage and current responses during the battery off time are highlighted in Fig. 13.

C. Simulation with the DG

In order to avoid battery SoC reaching the low limitation and insure the grid demand power requirement to be satisfied at any time, the diesel generator is added to the system. The DG unit will be triggered when the battery SoC is near the low limitation. The DG is supposed to provide a constant power of 500kW during the operation time. Figure 14 compares the different powers of the MCT system with BESS and DG. Figure 15 and 16 show the battery voltage/current and SoC variations respectively. It can be seen that the DG is triggered at 13:00 when the battery SoC is close to 0.1. Then DG is providing power to maintain the grid demand and the battery is charged by both DG and MCT power.

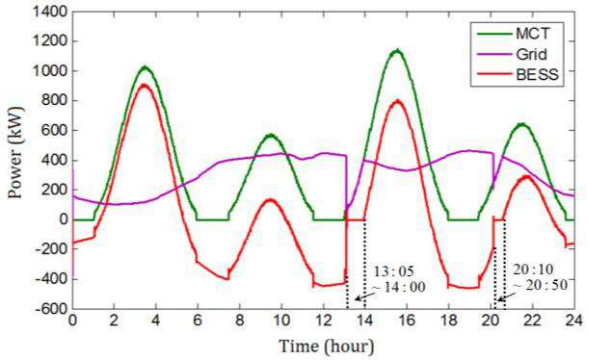

Fig. 12. Powers of the MCT system with BESS (initial SoC = 0.3).

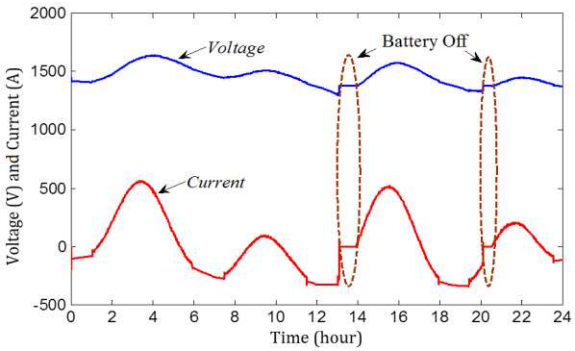

Fig. 13. BESS voltage and current (initial SoC = 0.3).

The DG is turned off when the battery power reaches the rated value at 14:40; after this point the MCT power is high enough to charge the battery and to provide grid demand power.

V. Conclusion

The MCT produced power varies greatly during one day period due to the variations of the tidal current speed. The vanadium redox flow battery is proposed to enable the MCT to provide demanded power to the grid. The grid demand reflects the load variation during one day. The battery model is developed considering various battery losses. Simulation is carried-out on a 1.5MW grid-connected MCT with a 3WMh flow battery. The simulation results for one day system operation validated the effectiveness of the battery model and its control strategy. The diesel generator is sized enough to supply the grid and restore the battery. The simulation shows the feasibility of the proposed daily power control scheme.

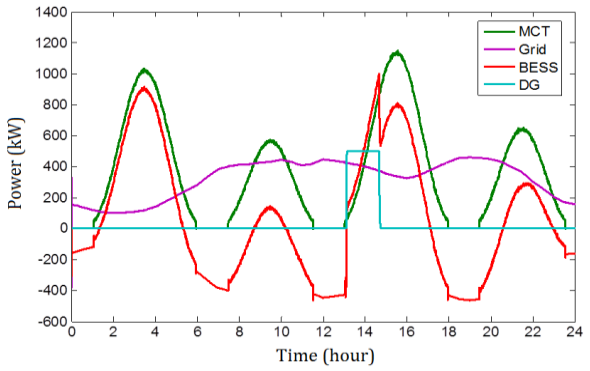

Fig. 14. Powers of the MCT system with BESS and DG.

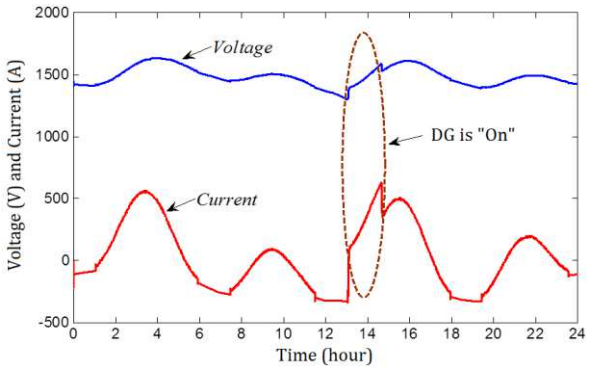

Fig. 15. BESS voltage and current.

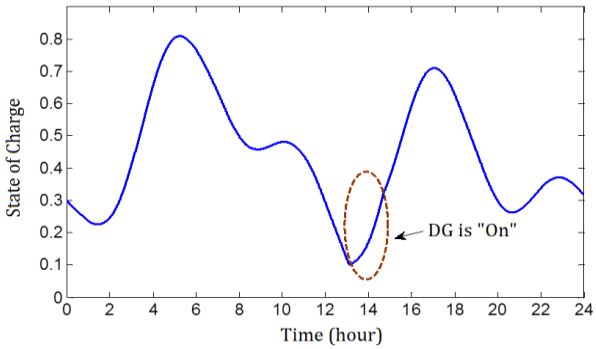

Fig. 16. SoC of the BESS.

The next step will be the sizing optimization of different system parts considering the global system cost.

TABLE I
PARAMETERS FOR THE VBR EQUIVALENT CIRCUIT

R_{fixed}	54.071 Ω
$R_{reaction}$	0.135 Ω
$R_{resistive}$	0.09 Ω
$C_{electrodes}$	0.0056 F
I_{pump} coefficient	0.0094

References

[1] A.S. Bahaj, "Generating electricity from the oceans," *Renewable and Sustainable Energy Review*, vol. 15, n°7, pp.3399-3416, Sept. 2011.

[2] S. Benelghali, M.E.H. Benbouzid and J. F. Charpentier, "Marine tidal current electric power generation technology: State of the art and current status," *in Proceedings of the 2007 IEEE IEMDC*, Antalya (Turkey), vol. 2, pp. 1407-1412, May 2007.

[3] S. Vazquez, S.M. Lukic, E. Galvan, L.G. Franquelo and J.M. Carrasco, "Energy storage systems for transport and grid applications," *IEEE Trans. Industrial Electronics*, vol. 57, n°12, pp.3881-3895, Dec. 2010.

[4] Z. Zhou, M.E.H. Benbouzid, J.F. Charpentier, F. Scuiller, and T. Tang, "A review of energy storage technologies for marine current energy systems," *Renewable and Sustainable Energy Review*, vol. 18, pp. 390-400, Feb. 2013.

[5] W. M. J. Batten, A. S. Bahaj, A. F. Molland, and J. R. Chaplin, "The prediction of the hydrodynamic performance of marine current turbines," *Renew. Energy*, vol. 33, no. 5, pp. 1085–1096, May 2008.

[6] J.G. Slootweg, S.W.H. de Haan, H. Polinder and W.L. Kling, "General model for representing variable speed wind turbines in power system dynamics simulations," *IEEE Trans. Power Systems*, vol. 18, n°1, pp.144-151, Feb. 2003.

[7] Z. Zhou, F. Scuiller, J.F. Charpentier, M.E.H. Benbouzid and T. Tang, "Power limitation control for a PMSG-based marine current turbine at high tidal speed and strong sea state," *in Proceedings of the 2013 IEEE IEMDC*, Chicago (USA), pp. 75-80, May 2013.

[8] B. Wu, B. Zhang, J. Wang, J. Li, *et al.* "Theoretical research for the application of flow storage battery in demand side management," *in Proceedings of the 2010 IEEE POWERCON*, Hangzhou (China), pp. 1-7, Oct. 2010.

[9] P. J. Hall and E. J. Bain, "Energy-storage technologies and electricity generation," *Energy Policy*, vol. 36, pp.4352-4355, 2008.

[10] J. Chahwan, C. Abbey and G. Joos, "VRB modeling for the study of output terminal voltages, internal losses and performance," *in Proceedings of the 2007 IEEE EPC*, Montreal (Canada), pp. 387-392, Oct. 2007.

[11] W. Li, G. Joós, and J. Bélanger, "Real-time simulation of a wind turbine generator coupled with a battery supercapacitor energy storage system," *IEEE Trans. Industrial Electronics*, vol. 57, n°4, pp.1137-1145, Apr. 2010.

[12] F. Caricchi, F. Crescimbini, F. Giulii Capponi and L. Solero, "Study of bi-directional buck-boost converter topologies for application in electrical vehicle motor drives," *in Proceedings of the 1998 IEEE APEC*, Anaheim (USA), vol. 1, pp. 287-293, Feb. 1998.